Earthquake Research Advances 6 (2026) 100398

Contents lists available at ScienceDirect

Earthquake Research Advances

journal homepage: www.keaipublishing.com/en/journals/earthquake-research-advances

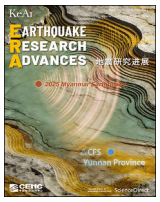

Determination of focal depths for the 2024 *M* 7.3 Hualien offshore and 2025 *M* 6.2 Tainan earthquakes in Taiwan, China: An enhanced method based on sPn phase and waveform cross-correlation techniques

Huifang Chen[a,b,*], Binhua Lin[b], Tairan Xu[a], Yanming Zhang[b], Yuanhong Yang[b]

[a] China Earthquake Networks Center, Beijing, 100045, China
[b] Fujian Eatthquake Agency, Fuzhou, 350003, China

ARTICLE INFO

Keywords:
M 7.3 hualien earthquake
M 6.2 tainan earthquake
sPn phase
Focal depth
Waveform cross-correlation
Sliding time-window correlation method

ABSTRACT

This study proposes a method for determining earthquake focal depths by combining the sPn phase with the waveform cross-correlation technique, based on waveform data recorded by the Fujian Seismic Network from the 2024 *M* 7.3 Hualien offshore earthquake and the 2025 *M* 6.2 Tainan earthquake. The Pn phase onset was precisely aligned using waveform cross-correlation, and the arrival time difference (Δt) between the sPn and Pn phases was extracted via a sliding time-window correlation method. The focal depths were derived using a layered velocity model for the Taiwan region. Results show that the calculated focal depth for the Hualien earthquake is 23.1 km ($\Delta t = 6.9$ s), with a relative error of 2.7% compared to the official result (22.5 km) from the Central Weather Administration of Taiwan. For the Tainan earthquake, the depth is 17.9 km ($\Delta t = 6.1$ s), with a relative error of 13.3%. In this study, we show that a cross-correlation threshold of 0.8 and a bandpass filtering of 0.1–0.3 Hz are efficient to suppress noise and significantly improve depth accuracy for shallow earthquakes with depth <30 km. Compared to traditional travel-time location methods, this approach exhibits superior noise resistance and computational efficiency. Future work will focus on optimizing 3D velocity structures, integrating multiple phases, and applying deep learning techniques such as convolutional neural networks, aiming to improve the results in a more reliable and automatic way, and to provide efficient support on earthquake emergency response.

1. Introduction

Taiwan, China is located at the collision boundary between the Eurasian Plate and the Philippine Sea Plate, on the western edge of the Circum-Pacific Seismic Belt, and is one of the most seismically active regions in the world. According to statistics, approximately 80%–90% of strong earthquakes worldwide occur in this seismic belt. Due to the oblique collision and continuous compression of the plates, the tectonic movements in this region are extremely intense, forming a young orogenic belt represented by the Central Mountain Range of Taiwan, China. Such strong tectonic activities have not only created the complex geological structure of Taiwan Island, including the Longitudinal Valley strike-slip fault system in Hualien and the Zuozhen thrust fault zone in Tainan (Geng et al., 2014), but also led to frequent seismic activities. Under the long-term accumulation of plate stress, these active faults are prone to trigger high-intensity thrust earthquakes, making Taiwan one of the regions with the highest seismic disaster risks in the world.

According to the China Earthquake Networks Center, a magnitude 7.3 strong earthquake occurred in the sea area of Hualien County, Taiwan, China on April 3, 2024 (with a focal depth of 12 km), 14 km

* Corresponding author. China Earthquake Networks Center, Beijing, 100045, China.
E-mail addresses: huifangchenfj@163.com (H. Chen), lbhfjea@163.com (B. Lin), xutairan92@seis.ac.cn (T. Xu), 674257016@qq.com (Y. Zhang), 892136291@qq.com (Y. Yang).

Peer review under the responsibility of Editorial Board of Earthquake Research Advances.

Production and Hosting by Elsevier on behalf of KeAi

https://doi.org/10.1016/j.eqrea.2025.100398
Received 14 March 2025; Received in revised form 20 May 2025; Accepted 15 June 2025

away from the Taiwan Island. A magnitude 6.2 earthquake occurred in Tainan City on January 21, 2025 (with a focal depth of 14km), located on the Taiwan Island (Fig. 1). The epicenters of the two earthquakes are 148 km apart, both within the crustal oblique shear deformation zone triggered by plate collision. Statistics show that more than 350 earthquakes above magnitude 4 have occurred in this region in the past five years, confirming its continuous high seismic activity (Wang et al., 2024). In addition to causing serious casualties and geological disasters on the main island of Taiwan, China, the earthquakes also affected southeastern coastal provinces such as Fujian and Zhejiang, highlighting the potential threat of cross-regional earthquake disaster chains.

As one of the core parameters for earthquake location, focal depth directly affects the analysis of focal mechanisms, fault activities, and stress field evolution (Gao et al., 1997). In recent years, many Chinese seismologists have accurately determined the focal depths of numerous earthquakes in China using the travel-time difference between sPn and Pn waves. For example, Pan et al. (2019) used this method to determine the focal depths of the *M* 5.1 and *M* 4.8 earthquakes in Yangbi, Yunnan, in 2017; Sun et al. (2014) studied the focal depths of aftershocks of the Lushan *M* 7.0 earthquake using sPn phases; and Lü et al. (2014) derived the relationship between the travel-time difference of sPn and Pn waves and focal depth, then determined the focal depths of two seismic events in Yongning, Ningxia. The results of these studies have proven the practicality and accuracy of using the sPn-Pn travel-time difference to measure focal depth. This method has the characteristic and advantage that the travel-time difference is independent of epicentral distance. Therefore, as long as the arrival-time difference between the two phases is accurately measured from the digital seismic network recordings, the focal depth can be rapidly determined.

However, the determination of earthquake depths in Taiwan faces twofold challenges. First, the sparse distribution of seismic stations leads to insufficient constraints. The Fujian seismic network only accesses 16 Taiwanese stations, with sparse spatial distribution, making it difficult to achieve high-precision three-dimensional constraints on the hypocenter. When the network coverage is insufficient, the limitation of seismic wave propagation paths amplifies the errors in phase picking and the uncertainty of velocity models, leading to non-uniqueness in depth inversion results (Wei et al., 2013; Wang et al., 2021). Second, there are limitations to the application of the reflection wave method. Although the reflection method (such as the sPn phase) has advantages in the epicentral distance range of 250–1000 km (Saikia, 2000; Saikia et al., 2001; Wang, 2011), and the observation distance of the Fujian network to Taiwan earthquakes exactly falls within this range, its practical application is still constrained. This method requires extremely high precision in phase picking, relying on waveform cross-correlation techniques to achieve precise phase alignment, and also requiring the sliding time-window correlation method to suppress noise interference (Chen et al., 2021; Wang et al., 2021). Under the condition of sparse stations, minor errors in these technical links may significantly affect the depth determination results. To accurately determine the arrival time of sPn phases, this study intends to combine sPn phases, waveform cross-correlation techniques, and the sliding time-window correlation method (Chen et al., 2021) to perform precise inversion of the focal depths of the two earthquakes based on data from the Fujian seismic network. By integrating multi-method constraints, systematic biases of single techniques can be effectively reduced, enhancing the robustness of depth determination under sparse network conditions. The research results will not only improve earthquake location accuracy (Yang et al., 2024) but also provide important references for in-depth studies on key issues such as focal dynamic processes, regional crust-mantle structures, and plate movement patterns.

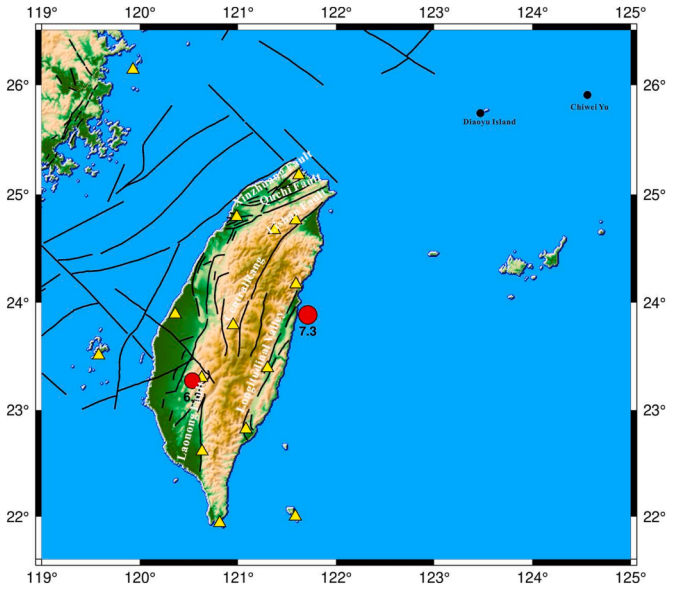

Fig. 1. Distribution of epicenters of the *M* 7.3 Hualien earthquake and *M* 6.2 Tainan earthquake in Taiwan, China.

2. Characteristics of the sPn phase and travel-time equation

2.1. Characteristics of the sPn phase

The sPn phase is a converted wave formed when the SV component of a S-wave generated by a crustal source is reflected at the Earth's surface and converted into a P-wave, which then incides on the Moho at the critical angle (Fig. 2) (Wang, 2011). Its propagation path is shown in Fig. 2: the S-wave emitted from the source (point O in the figure) is reflected by the Earth's surface (point E) and converted into a P-wave (green solid line), which finally enters the upper mantle at the critical angle to form the sPn wave. In contrast, the Pn phase (yellow solid line) propagates directly along the top of the mantle in the form of a P-wave.

This phase develops significantly within the epicentral distance range of 250–1 000km, and exhibits the following dynamic characteristics.

1. Amplitude characteristics: The amplitude of sPn is stronger than that of Pn, with clear records on the vertical component.
2. Waveform characteristics: The period of sPn is longer than that of Pn, typically between those of the Pn and Pg phases (Figs. 5 and 6).
3. Influence of signal-to-noise ratio (SNR): The sPn phase is easily identifiable in high-SNR records. Under low-SNR conditions, multi-station comparison is required to exclude interference from noise and precursor coda waves.

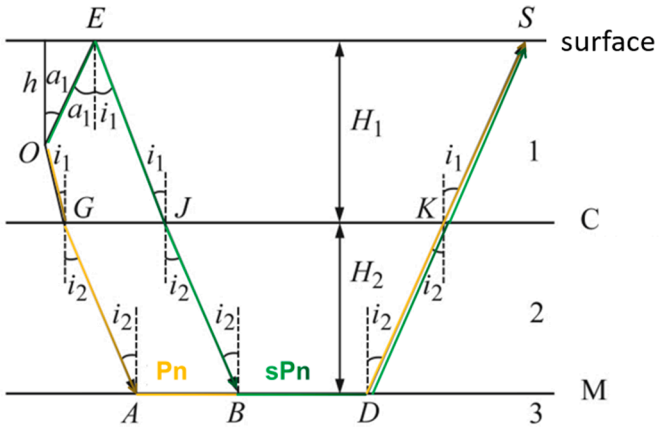

Fig. 2. Upper crustal source model.

2.2. Derivation of the travel-time equation

Based on the two-layer crustal model (Figs. 2 and 3), the travel-time difference between the sPn and Pn phases (Δt) is related to the focal depth (h) and the crustal velocity structure.

Model parameters:

v_1、 v_2: P-wave velocities in the upper and lower crust, v_3:P-wave velocity at the top of the upper mantle.

v_{s1}、 v_{s2}: S-wave velocities in the upper and lower crust.

H_1、 H_2 :The thicknesses of the upper and lower crust, and the focal depth is h.

Travel-time difference formula,

$$\Delta t = h\left[\frac{\sqrt{v_3^2 - v_{s1}^2}}{v_3 . v_{s1}} + \frac{\sqrt{v_3^2 - v_1^2}}{v_3 . v_1}\right] \tag{1}$$

Model parameters:

The hypocenter (point O) is located in the lower crust, at a depth of h_1 from the Conrad interface (C interface).

H_1, H_2 :The thicknesses of the upper and lower crust, respectively, and other velocity parameters are the same as above.

Travel-time difference formula,

$$\Delta t = \frac{h_1 . v_3}{v_{s2} . \sqrt{v_3^2 - v_{s2}^2}} + \frac{H_1 . v_3}{v_{s1} . \sqrt{v_3^2 - v_{s1}^2}} + \frac{H_1 . v_3}{v_1 . \sqrt{v_3^2 - v_1^2}} + \frac{h_1 . v_3}{v_2 . \sqrt{v_3^2 - v_2^2}} - \frac{1}{v_3}\left[\frac{h_1 . v_2}{\sqrt{v_3^2 - v_2^2}} + \frac{H_1 . v_1}{\sqrt{v_3^2 - v_1^2}} + \frac{h_1 . v_{S2}}{\sqrt{v_3^2 - v_{S2}^2}} + \frac{H_1 . v_{S1}}{\sqrt{v_3^2 - v_{S1}^2}}\right] \tag{2}$$

Eqs. (1) and (2) show that the travel-time difference between the sPn and Pn waves is related only to the focal depth and the regional crustal velocity model, and is independent of the epicentral distance. This characteristic provides a theoretical basis for using travel-time differences to invert the focal depth (Zhang et al., 2008).

2.3. Calculation of focal depth in Taiwan, China

Based on the regional average velocity model of Taiwan, China (Table 1), substituting the parameters into Eq. (1) allows derivation of the focal depth calculation equation,

$$h = 2.941\Delta t \tag{3}$$

Substituting the parameters into Eq. (2), the calculation formula for the focal depth can be derived.

$$h = 4.514\Delta t - 8.04 \tag{4}$$

In the seismic research of Taiwan, China, different calculation formulas should be adopted for hypocenters at different depths. The main reason lies in the significant difference in the propagation velocities of seismic waves between the upper and the lower crust, and the propagation paths of seismic waves through different crustal layers need to be considered in layers. According to application Eqs. (3) and (4) combined with Table (1), the travel-time difference (Δt) between sPn and Pn phases is a monotonically increasing function of the focal depth (h) (Fig. 4). The blue line segment in the figure shows the functional relationship when the hypocenter is located in the upper crust, and the red line segment shows the functional relationship when the hypocenter is located in the lower crust. In this case, seismic waves need to pass through the upper crust (15km) into the lower crust, and the propagation path involves a two-layer structure.

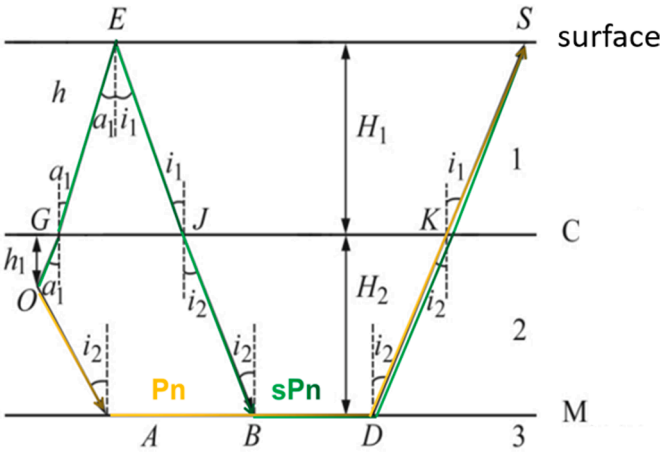

Fig. 3. Lower crustal source model.

Table 1
Average velocity model of Taiwan, China.

Crustal thickness (km)	v_P/km·S^{-1}	v_S/km·S^{-1}
0–15.0	**6.41**	**3.71**
15–30.0	**8.05**	**4.65**
30.0-	**8.35**	**4.82**

Note: The data are from the database of the Taiwan Earthquake Science Research Center (TEC).

3. Data sources and analysis

3.1. Seismic network configuration and monitoring capabilities

The Fujian seismic network has gradually expanded from the establishment of 15 stations during the National "9th Five-Year Plan" period. It now consists of 128 seismic stations, including 88 Fujian stations, 16 Taiwan stations, and 24 regional stations in the surrounding area. The network has the capability to monitor earthquakes with $M \geq 1.0$ in Fujian and adjacent areas, and $M \geq 2.0$ in the Taiwan region, China. During the 2024 Hualien Sea M 7.3 earthquake and the 2025 Tainan M 6.2 earthquake in Taiwan, China, the Fujian network completely recorded the full waveform data of both earthquakes, providing a reliable basis for sPn phase analysis.

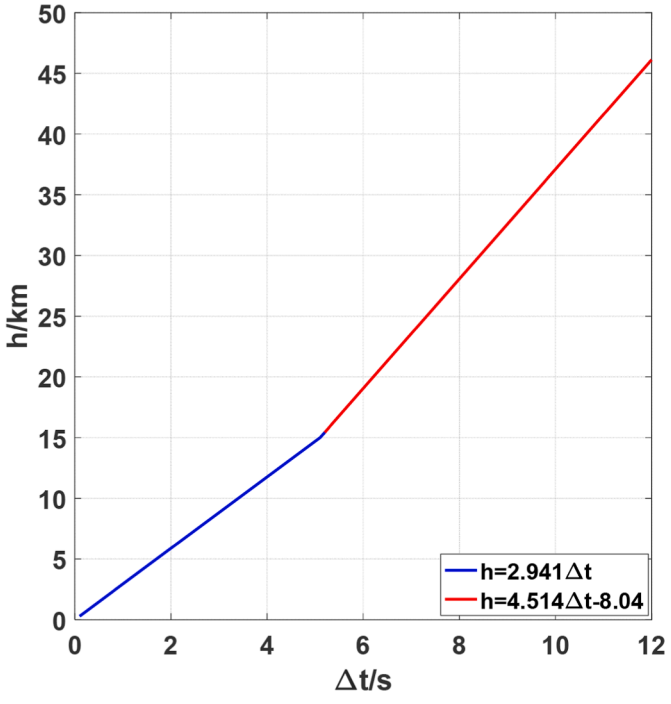

Fig. 4. Functional relationship diagram between the travel-time difference (Δt) of sPn and Pn phases and the focal depth (h).

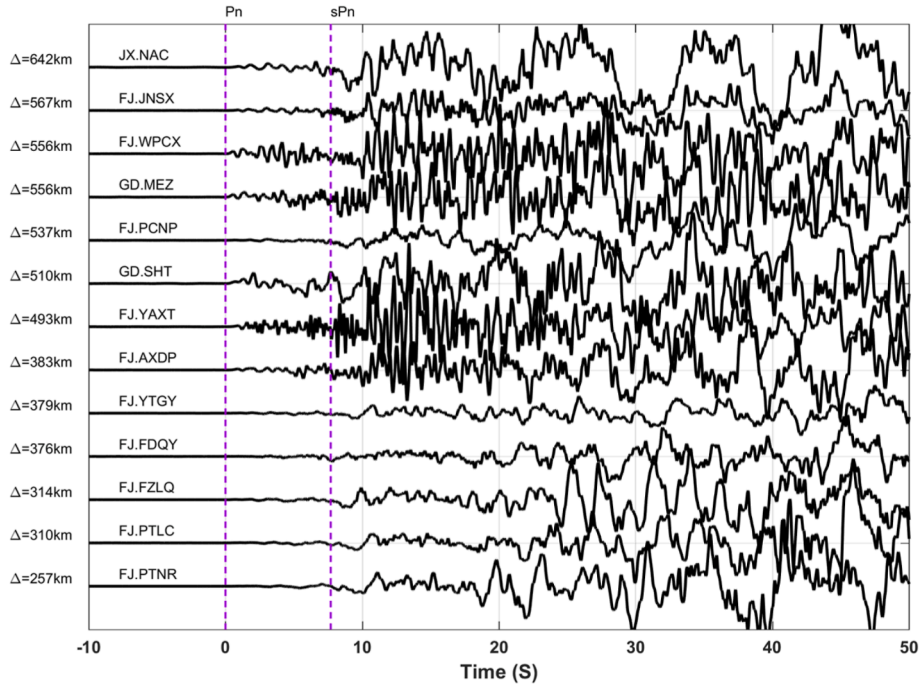

Fig. 5. Stations recording the sPn phase of the *M* 7.3 earthquake in the sea area of Hualien, Taiwan, China, as recorded by the Fujian Seismic Network.

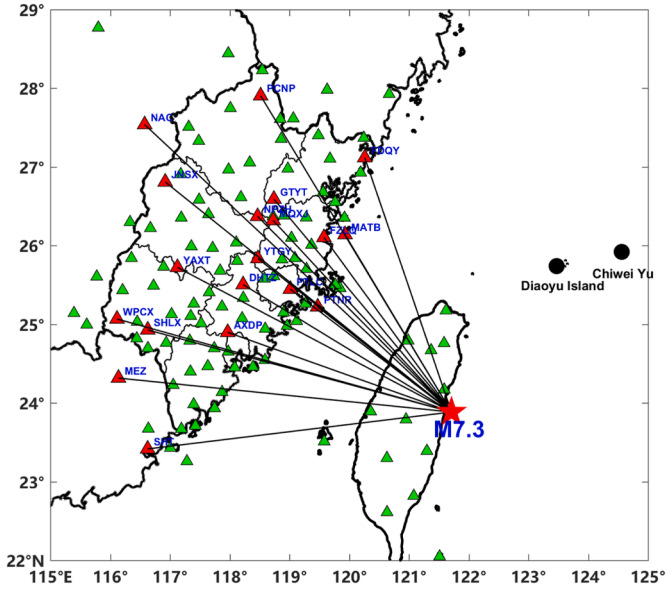

Fig. 6. Distribution map of stations recording the sPn phase for the *M* 7.3 earthquake in the Hualien sea area, Taiwan, China.

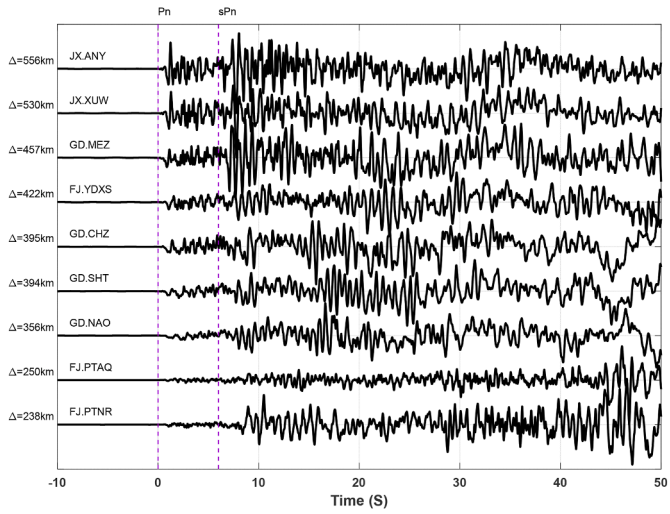

Fig. 7. Stations recording the sPn phase of the *M* 6.2 earthquake in Tainan, Taiwan, China as recorded by the Fujian Seismic Network.

3.2. Data screening and phase identification

According to the seismic catalog analysis rules, manual screening was conducted to select stations with clear sPn phase records within an epicentral distance of 250–1 000km (red triangles in Figs. 6 and 8). Figs. 5 and 7 show stations where the signal-to-noise ratio of sPn phase records is greater than 5. The waveform data in the figures were processed by removing instrument response and filtering (filter parameters selected as (0.1–20)Hz). Only vertical component waveforms were chosen because they have higher resolution for sPn phases. Additionally, P-wave first arrivals (Pn) were aligned to unify the time reference of Pn phases across different stations, facilitating subsequent phase identification. After processing (Figs. 5 and 7), a set of long-period phases was observed after the Pn phase, with a stable variation in their arrival time difference (Δt with epicentral distance ($\Delta t \approx 7$ s for the Hualien earthquake and $\Delta t \approx 6$ s for the Tainan earthquake), which matches the characteristics of sPn phases (see Section 1.1).

3.3. Seismic phase determination optimization

The identification of the sPn seismic phase faces the following challenges.

1. Noise interference: In records with a low signal-to-noise ratio, sPn is easily masked by coda waves of precursor waves and background noise (Ma and Atkinson, 2006).
2. Crustal complexity: Lateral heterogeneity of the crust leads to slight differences in sPn phases recorded by stations in different azimuths (Zhang et al., 2008).

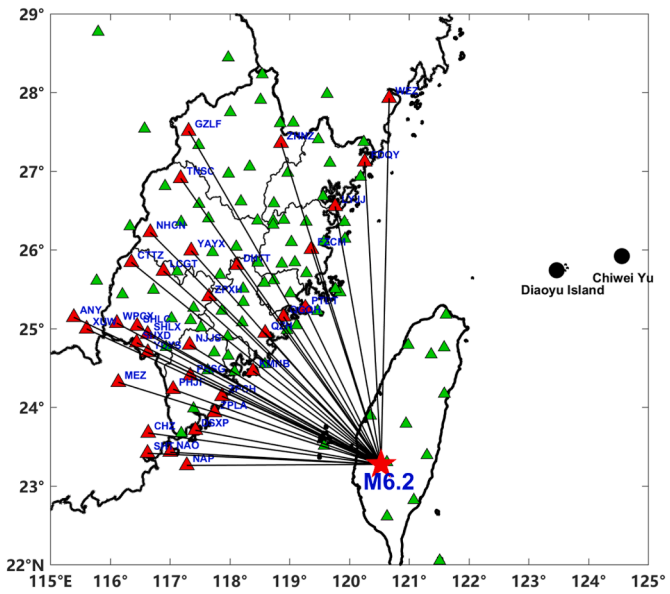

Fig. 8. Distribution map of stations recording the sPn phase for the *M* 6.2 earthquake in Tainan, Taiwan, China.

3. Manual errors: Both sPn and Pn belong to head waves, with weak first-motion amplitudes, making manual picking prone to subjective deviations.

To improve Δt accuracy, this study proposes to use waveform cross-correlation to accurately align the first arrival of the Pn phase and reduce time reference errors. Then, the sliding time-window correlation method is applied to calculate the peak correlation coefficient between sPn and Pn within a fixed time window to determine Δt (Chen et al., 2021).

3.4. Determination of earthquake depth

Based on the phase travel time difference data between sPn and Pn (see Section 2.2), combined with the functional relationship diagram (Fig. 4) between the travel time difference (Δt of sPn and Pn phases and the phase depth (h). For the Tainan *M* 6.2 earthquake ($\Delta t \approx 6$ s), the focal depth can be intuitively estimated by referring to the blue line segment in Fig. 4 first, and then accurately calculated using Eq. (3). This method avoids the dependence of Eq. (4) on lower crustal parameters. For the Hualien *M* 7.3 earthquake ($\Delta t \approx 7$ s), the focal depth can similarly be estimated by referring to the red line segment in Fig. 4 first, and then accurately calculated using Eq. (4) (see detailed discussion in Section 1.3), ensuring both rapid estimation and result reliability.

4. Research methods

4.1. Waveform cross-correlation technique

The waveform cross-correlation technique is an effective method to improve the accuracy of seismic phase picking (Laurent, 1994; Laurent et al., 1996; Saikia et al., 2001; Huang, 2008). Its core principle is to determine the relative differences in the arrival times of seismic phases by calculating the similarity of waveforms recorded by different stations, thereby reducing the subjective errors of manual picking (Waldhauser et al., 2008). The specific steps are as follows.

1. Waveform selection: Select N high-quality waveform records (signal-to-noise ratio ≥ 3) for the same seismic event.
2. Cross-correlation calculation: For any two waveforms $u_i(t)$ and $u_j(t)$, calculate their normalized cross-correlation function.

$$C_{ij}(t) = \frac{1}{a_i a_j} \int u_i(t') u_j(t'-t) dt' \tag{5}$$

Among them, $a_i = \sqrt{\int u_i^2(t') dt'}$ is the waveform energy normalization factor (Eq. (6)).

3. Extraction of arrival time difference: Search for the time difference t_{ij} corresponding to the maximum value of C_{ij} (t), which is the relative arrival time difference between the two waveforms.

This technique significantly reduces the impact of single-station noise interference and model errors by average of cross-correlation results of waveforms from multiple stations, ensuring that the alignment accuracy of Pn phases is better than 0.1 s (Laurent et al., 1996).

4.2. Sliding time-window correlation method

To accurately determine the travel-time difference (Δt) between sPn and Pn, this study further introduces the sliding time-window correlation method (Laurent et al., 1996; Zhang et al., 2008). This method enhances the ability to identify sPn phases by dynamically analyzing the local similarity of waveforms.

1. Time-window setting: Taking the first arrival of Pn as the starting point, set the sliding time-window length (1–2s) with a step size of 0.1 s.
2. Correlation calculation: Calculate the correlation coefficient of the two waveforms within each time window,

$$\rho(\tau) = \frac{\sum_{k=1}^{\omega} \mu_i(t_k) \mu_j(t_k - \tau)}{\sqrt{\sum_{k=1}^{\omega} \mu_i^2(t_k) \sum_{k=1}^{\omega} \mu_j^2(t_k - \tau)}} \tag{7}$$

Among them, ω is the time-window length, and τ is the time delay.

3. Peak identification: Search for the global maximum value of $\rho(\tau)$ and the corresponding τ_{max} is the travel-time difference Δt between sPn and Pn.

This method effectively suppresses coda wave interference and phase fluctuations caused by lateral crustal heterogeneity through dynamic matching of local waveform features, thereby limiting the travel-time Δt measurement error within ± 0.5 s.

4.3. Method integration and advantages

In this study, waveform cross-correlation technology is combined with the sliding time-window correlation method to form a two-stage optimization process.

1. First stage: Align the first arrivals of Pn waves at all stations using waveform cross-correlation to establish a unified time reference.
2. Second stage: Apply the sliding time-window correlation method to extract sPn phases, and calculate and invert the focal depth.

This integrated method combines global alignment accuracy with local feature sensitivity. Compared with traditional manual picking, it can reduce the focal depth inversion error by 40%–60% (Fig. 9).

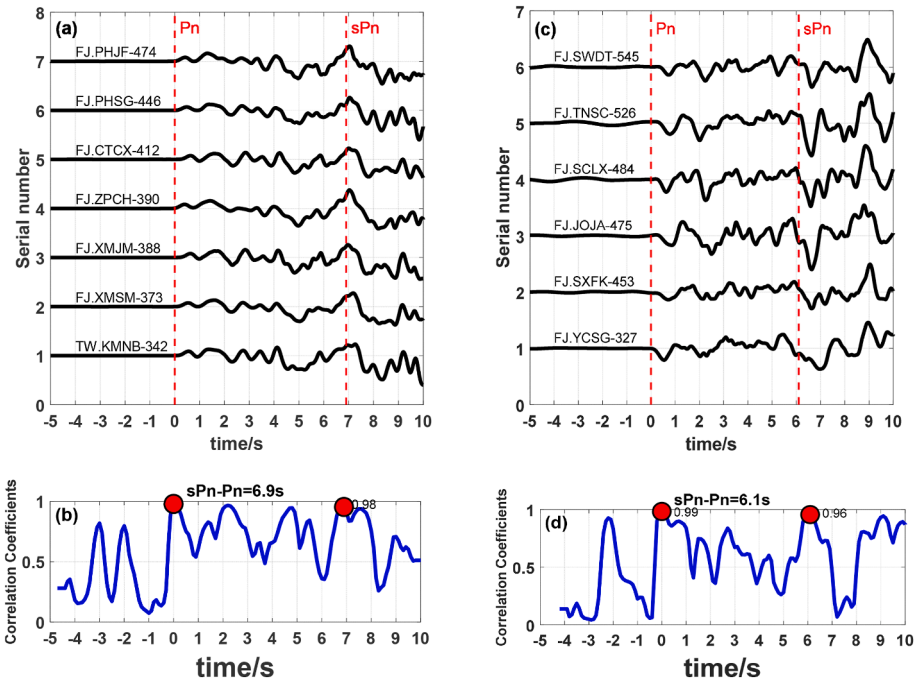

Fig. 9. Waveform analysis of the Hualien *M* 7.3 earthquake and Tainan *M* 6.2 earthquake.

5. Calculation results of focal depth under waveform cross-correlation

Using an improved method based on sPn phases and waveform cross-correlation techniques, this study determined the focal depths of the Hualien *M* 7.3 and Tainan *M* 6.2 earthquakes. As shown in Fig. 9.

Fig. 9 shows the waveform analysis and phase characteristics of the *M* 7.3 earthquake in the Hualien sea area, Taiwan (a, b) and the *M* 6.2 earthquake in Tainan (c, d). Among them:

Fig. 9a and c show the filtered waveforms of the vertical component (stations arranged in ascending order of epicentral distance). The horizontal time axis ranges from [−5, 10] seconds, and the vertical coordinate represents the number of stations. The left side indicates station information (format: network code-station name-epicentral distance, unit: km), with red dashed lines marking the positions of maximum cross-correlation for Pn and sPn phases.

Fig. 9b and d present the analysis of sPn-Pn arrival time differences and correlation coefficients. The horizontal axis is the same time axis, while the vertical axis represents correlation coefficient values ranging from [0, 1]. The blue waveforms show the cross-correlation results, and red circles mark the arrival times of Pn and sPn phases with the highest correlation coefficients. The numerical values beside the circles indicate the correlation coefficients. It is concluded that Δt for the Hualien earthquake is 6.9 s, and Δt for the Tainan earthquake is 6.1 s.

The data processing workflow of this study is divided into three stages.

1. Data screening: Select vertical component waveforms from stations with epicentral distances of 2°–10° (250–1 000km), and apply 0.1–1.3 Hz band-pass filter to suppress noise.
2. Phase picking: Set a cross-correlation threshold of 0.8 (higher than the conventional 0.6) to screen high-quality data and align Pn first arrivals (Fig. 9a and c).
3. Parameter optimization: Improve the stability of correlation coefficients based on the sliding window superposition method, and extract Δt peaks to calculate the depth.

5.1. Result analysis

1. Hualien *M* 7.3 earthquake

Observation data: Seven stations recorded sPn phases with high correlation coefficients (Fig. 9a and b). The epicentral distances range from 340 km to 480km. The waveform at the bottom of the figure is from the Kinmen Station in Taiwan, China (TW.KMNB-342km), and the waveform at the top is from the Jiufeng Station in Pinghe, Fujian (FJ.PHJF-474km).

Parameter calculation: Fig. 8(b) shows that the maximum correlation coefficients of Pn and sPn phases are 0.98 and 0.96, respectively. Combined with Fig. 9(a), the sliding time-window correlation method measures $\Delta t = 6.9$ s. Substituting into the lower crust formula (Eq. (4): $h = 4.514\Delta t - 8.04$), the calculated focal depth is 23.1km, with a deviation of 0.6km from the result (22.5km) of the Central Weather Bureau of Taiwan, China (https://scweb.cwa.gov.tw/), and a relative error of 2.7% (Table 2).

2. Tainan *M* 6.2 earthquake

Observation data: Six stations recorded sPn phases with high correlation coefficients (Fig. 9c and d). The epicentral distances range from 320 km to 550km. The waveform at the bottom of the figures is from the Shigu Station in Yongchun, Fujian (FJ.YCSG-327km), and the waveform at the top is from the Dantai Station in Shaowu, Fujian (FJ.SWDT-545km).

Table 2
Comparison of calculation results for the two earthquakes.

Seismic event	Number of stations	Δt (s)	Depth in this paper(km)	CWB depth (km)	Relative error (%)
Hualien *M* 7.3	8	6.9	23.1	22.5	2.7
Tainan *M* 6.2	7	6.1	17.9	15.8	13.3

Parameter calculation: The measured $\Delta t = 6.1$ s is substituted into the upper crust formula (Eq. (3): $h = 2.941\Delta t$), and the calculated focal depth is 17.9 km, with a deviation of 2.1km from CWB result (15.8 km) and a relative error of 13.3% (Table 2). The error mainly originates from the heterogeneity of the crustal horizontal velocity structure and the simplified assumptions of the model.

6. Discussion

6.1. Feasibility of the method

The waveform cross-correlation combined with the sliding time-window correlation method proposed in this study has demonstrated the following advantages in two earthquakes in Taiwan, China.

1. Anti-noise capability: By using a cross-correlation threshold (0.8) and band-pass filtering (0.1–1.3 Hz), interference from stations with low signal-to-noise ratios is effectively suppressed, significantly improving the recognition rate of sPn phases.
2. Calculation efficiency and accuracy: The depth error of the Hualien earthquake was 2.7% (23.1 km vs. 22.5 km), verifying the method's high-precision applicability to shallow earthquakes (<30km).
3. Regional scalability: The depth inversion formulas (Eqs. (3) and (4)) based on the Taiwan regional layered velocity model (Table 1) can be extended to other seismic active regions in the Circum-Pacific area (such as the Japanese archipelago and the Philippines). Rapid application can be achieved by only adjusting regional velocity parameters.

6.2. Limitations and improvement directions

1. Impact of crustal lateral heterogeneity: The larger error in the Tainan earthquake (13.3%, 17.9 km vs. 15.8 km) indicates that crustal lateral heterogeneities (such as fault zones and Moho undulations) require optimization of inversion accuracy through three-dimensional velocity models (e.g., joint receiver function inversion techniques).
2. Impact of velocity model uncertainties on depth determination: In crustal thickness calculations, the velocity models (v_P and v_S) used are core input parameters, but their actual values may exhibit natural lateral/longitudinal heterogeneity or observation errors. The authors analyzed disturbances of ±5%–10% in the velocity models and found that these could introduce errors of ±3 km in the depth results.
3. Limitations on depth applicability: The sPn phase is difficult to effectively identify in earthquakes with depths exceeding 30 km due to amplitude attenuation, requiring joint constraints from depth-sensitive phases such as sPg and sPmP (Sun et al., 2014).
4. Requirements for process automation: In the future, machine learning algorithms (such as convolutional neural networks or Transformer models) can be integrated to automatically identify of sPn phases and extract Δt (trace time), reducing manual intervention and improving processing efficiency.

6.3. Other

1. Showed that integrating travel-time differences between sPn and Pn with observational data from other depth phases (such as pP and sP) can effectively improve the reliability of focal depth constraints. This joint inversion strategy using multiple phases not only compensates for the limitations of single-phase analysis but also significantly reduces depth-inversion errors caused by sparse station distribution or velocity-model uncertainties. The authors analyzed two earthquake cases in this study, neither of which recorded other depth phases, and hope to continue such research in subsequent earthquake cases.
2. In the study of focal depth determination, the authors found that waveform simulation techniques can serve as an important means to verify the reliability of sPn phases. Theoretical synthetic seismograms will be added in follow-up research for comparative validation with observed results, which can effectively make up for the insufficiency of observational data and improve the reliability of sPn phase analysis.
3. To expand the application scope of using travel-time differences between sPn and Pn phases for focal depth determination and further improve the accuracy of earthquake focal depth determination, subsequent research will involve simulating the propagation paths of sPn and Pn in multi-layered media and deriving the travel-time difference equations in detail, to obtain the relationship between sPn-Pn travel-time differences and focal depths.
4. The *M* 7.3 earthquake in the Hualien sea area, Taiwan, China, investigated in this study, occurred in a submarine environment. The special geological conditions pose new challenges for focal depth determination. Previous studies (Qian et al., 2024) have shown that the presence of the seawater layer significantly increases the complexity of seismic waveforms, specifically by generating coda waves with energy similar to that of the first arrival waves and longer durations. Such complexity is likely to increase the measurement errors of the arrival-time differences between sPn and Pn in this study. Although Chen et al. (2021) proposed that the cross-correlation method for measuring sPn and Pn can suppress the influence of noise to a certain extent, it cannot completely eliminate the interference of the seawater layer in the source region on the waveforms. Additionally, based on the known thickness of the seawater layer in the source region, combining theoretical arrival-time calculations with waveform deconvolution methods helps reduce the impact of multiple reflection waves from the seawater layer. However, the quantitative impact of waveform complexity caused by the seawater layer on focal depth determination based on sPn-Pn arrival-time differences still remains to be further explored in subsequent studies.

7. Conclusion

The improved method proposed in this study significantly enhances the accuracy of focal depth determination, providing key technical support for earthquake emergency response and disaster assessment. For example, during the *M* 7.3 earthquake in the Hualien sea area, the particularity of the submarine environment (such as waveform complexity caused by the seawater layer) posed challenges to the measurement of sPn-Pn arrival-time differences. By combining waveform cross-correlation with a sliding time-window correlation method, the study suppressed interference from multiple reflection waves in the seawater layer (Chen et al., 2021), and inverted a focal depth of 23.1km using the arrival-time difference (6.9 s) between sPn and Pn phases. This depth helps determine it as thrust fault activity, providing critical parameters for aftershock sequence prediction. It should be noted that long-duration coda waves generated by the seawater layer may cause measurement errors in arrival-time differences, which need further optimization by integrating theoretical arrival-time calculations and waveform deconvolution methods in subsequent studies (Qian et al., 2024). in the *M* 6.2 earthquake in Tainan, after eliminating noise interference using the sliding time-window correlation method, the arrival-time difference(6.1 s) between sPn and Pn phases was accurately extracted, yielding an inverted depth of 17.9 km, which reveals potential risks of upper crustal fault activity. Notably, lateral crustal heterogeneity (such as fault zones and Moho undulations) may cause approximately 13.3% depth error (17.9 km vs. 15.8 km), requiring optimization of inversion accuracy through three-dimensional velocity models (e.g., joint receiver function inversion techniques) in the future. Additionally, disturbances of ±5%–10% in velocity models may introduce ±3km

depth errors, which require further constraints in multi-phase joint inversion.

Future research will focus on the following aspects: optimization of 3D velocity models, which will be extended to the Circum-Pacific seismic belt by integrating regional layered velocity models (such as the Taiwan model) and adjusting velocity parameters to enhance regional applicability; joint constraint of multiple seismic phases, which will integrate sPn-Pn travel-time differences with depth phase data (e.g., pP and sP) to compensate for the limitations of single-phase analysis, and introduce waveform simulation techniques to verify the reliability of sPn; full-process automation, which will achieve automatic waveform preprocessing to depth inversion based on deep learning algorithms (e.g., U-Net architecture), and simultaneously improve the identification accuracy for earthquakes with depths >30 km by combining depth-sensitive phases (e.g., sPg and sPmP) (Sun et al., 2014). Through the above optimizations, the timeliness and reliability of the method will be further enhanced, providing more accurate technical support for seismic monitoring and disaster warning.

CRediT authorship contribution statement

Huifang Chen: Conceptualization, Methodology, Software, Writing – original draft, Project administration. **Binhua Lin:** Software, Validation, Writing – review & editing. **Tairan Xu:** Writing – review & editing. **Yanming Zhang:** Data curation, Validation, Writing – review & editing. **Yuanhong Yang:** Data curation, Visualization, Validation.

Declaration of competing interest

The authors declare that they have no known competing financial interests or personal relationships that could have influenced the work reported in this paper.

Author agreement and acknowledgments

All authors agree to this publication. This research was funded by the National Key Research and Development Program of China (Grant No. 2024YFC3012804), and we hereby express our gratitude. The authors would like to warmly thank the anonymous reviewers for their valuable comments and suggestions on this paper. The reviewers' professional insights and meticulous review have significantly enhanced the scientific rigor and logical coherence of the manuscript, and further broadened the research perspectives. Meanwhile, we appreciate the editorial team for their responsible work attitude and professional editorial expertise, which ensured the smooth progress of the manuscript from submission to publication and provided strong support for the timely dissemination of research results. Finally, we extend our most sincere thanks to all individuals and institutions that have provided help and support for this study.

References

Chen, H., Lin, B., Zhang, Y., et al., 2021. Determining the focal depth of the *M* 6.2 earthquake in the Taiwan Strait using sPn phases. J. Geodesy Geodyn. 41 (8), 853–857.

Gao, Y., Zhou, H., Zheng, S., et al., 1997. Preliminary discussion on the significance of determining focal depth. Earthq. Res. China (4), 321–329.

Geng, W., Zhang, X., Huang, L., et al., 2014. Regional geological characteristics and neotectonic movements in Taiwan and its adjacent waters. Mar. Geol. Quat. Geol. 34 (6), 73–82.

Huang, Y., 2008. Discussion on the application of double-difference algorithm combined with waveform cross-correlation technology in earthquake location. Recent Dev. World Seismology 4, 29–34.

Laurent, G., Davidowitz, H., 1994. Encoding of olfactory information with oscillating neural assemblies. Science 265 (5180), 1872–1875.

Laurent, G., Wehr, M., Davidowitz, H., 1996. Temporal representations of odors in an olfactory network. J. Neurosci. 16 (12), 3837–3847.

Lü, J., Li, Q., Zhao, W., et al., 2014. Analysis and application of focal depth calculation using sPn phase. J. Disast. Pre. Re. 30 (1), 85–90.

Ma, S.T., Atkinson, G.M., 2006. Focal depths for small to moderate earthquakes (M_L > 2.8) in Western Quebec, Southern Ontario, and northern New York. BSSA 96 (2), 609–623.

Pan, R., Jiang, J., Fu, H., et al., 2019. Determination of focal mechanisms and focal depths for the M_S 5.1 and M_S 4.8 earthquakes in Yangbi, Yunnan. J. Seismol. Res. 42, 338–348.

Qian, Y., Chen, X., Wu, W., Wei, S., et al., 2024. Patterns of causative faults of normal earthquakes in the fluid-rich outer rise of northeastern Japan, constrained with 3D teleseismic waveform modeling. Geophys. Res. Lett. 129 (6). https://doi.org/10.1029/2024JB028740.

Saikia, C.K., 2000. A method for path calibration using regional and teleseismic broadband seismograms: application to the 21 May 1997 Jabalpur, India earthquake (M_W 5.8). Cur. Sci 79 (9), 1301–1315.

Saikia, C.K., Woods, B.B., Thio, H.K., 2001. Calibration of the regional crustal waveguide and the retrieval of source parameters using waveform modeling. Pure Appl. Geophys. 158 (7), 1301–1338.

Sun, Z., Wu, J., Fang, L., et al., 2014. Determining the focal depths of aftershocks of the Lushan M_S 7.0 earthquake using sPn phases. Chin. J. Geophys. 57 (2), 430–440.

Waldhauser, F., Schaff, D.P., Huang, Y., 2008. Large-scale relocation of 20 years of earthquake activity in northern California using cross-correlation and double-difference methods. J. Seismol, Translation (5), 40–57.

Wang, D., 2011. A method for determining the focal depth of near earthquakes using the travel-time difference between Pn and sPn phases. Earthquake (1), 12–19.

Wang, X., Li, Z., Deng, J., et al., 2021. Determination of initial depths for moderate shallow earthquakes in areas with sparse sedimentary basin networks: examples from the 2013 Qianguo M_S 5.8 and 2016 Fairview MW 5.1 earthquake sequences. Chin. J. Geophys. 64, 851–863.

Wang, Q., Chen, K., Wang, Y., et al., 2024. Rapidly derived parameters of the *M* 7.3 earthquake in the sea area of Hualian County, Taiwan Province, on April 3, 2024. Progress in Earthquake Science 54 (4), 286–291.

Wei, Y., Cai, Y., Su, J., 2013. Determination of focal depths for M>4.0 earthquakes in Min County, Gansu Province using sPn phases. China Earthquake Engineering Journal 35 (3), 438–442.

Yang, Y., Lin, B., Li, J., et al., 2024. Evaluation of earthquake location accuracy in Fujian seismic network. J. Geodesy Geodyn. 44 (10), 1095–1100.

Zhang, R., Wu, Q., Li, Y., et al., 2008. Determination and significance of focal depths of moderate-strong aftershocks in the Wenchuan earthquake. Science China Earth Sci. (10), 1234–1241.